The Heat Capacities of Thermomiotic ScF_3 and ScF_3-YF_3 Solid Solutions

Carl P. Romao (cpr@dal.ca),[1] *Cody R. Morelock* (cody.morelock@gatech.edu),[2] *Michel B. Johnson* (mbjohnso@dal.ca),[1] *J. W. Zwanziger* (jzwanzig@dal.ca),[1] *Angus P. Wilkinson* (angus.wilkinson@chemistry.gatech.edu),[2,3] *and Mary Anne White* (mary.anne.white@dal.ca)[1,*]

[1] Department of Chemistry and Institute for Research in Materials, Dalhousie University, Halifax, Nova Scotia, B3H 4R2, Canada

[2] School of Chemistry and Biochemistry, Georgia Institute of Technology, Atlanta, Georgia 30332, United States

[3] School of Materials Science and Engineering, Georgia Institute of Technology, Atlanta, Georgia 30332, United States

[*] Corresponding author. Tel: +1-902-494-6538;

E-mail address: mary.anne.white@dal.ca (Mary Anne White)

ABSTRACT

ScF_3 exists in a cubic ReO_3 structure that exhibits negative thermal expansion (NTE) from 10 K to 1100 K, while substituted $Sc_{1-x}Y_xF_3$ materials display the same behaviour at room temperature but transition into positive thermal expansion rhombohedral phases upon cooling. We have measured the heat capacity of ScF_3 from 0.4 to 390 K and found no evidence of a phase transition, but do find that its low-temperature heat capacity is anomalously high. The heat capacities of substituted $Sc_{1-x}Y_xF_3$ materials are also reported and show evidence of the cubic-rhombohedral phase transition for $x \geq 0.1$ and smaller anomalies in the low-temperature heat capacity of the positive thermal expansion rhombohedral phases. To aid in interpretation of these results, the heat capacity of ScF_3 was calculated from its phononic structure using density functional theory.

KEYWORDS

Negative thermal expansion, thermomiotic, heat capacity, ceramics, solid solutions

Introduction:

Scandium trifluoride (ScF_3) belongs to the category of thermomiotic materials, also known as negative thermal expansion (NTE) materials [1]. The coefficient of thermal expansion (CTE) of ScF_3 has been reported to be negative over a wide temperature range (10 K to 1100 K) [2]. ScF_3 has the cubic ReO_3 structure, which consists of corner-sharing ScF_6 octahedra. NTE in ScF_3 arises from transverse vibrations of the F atoms, which shorten the average Sc–Sc distance [2,3]. Recently, the thermal expansivities and compressibilities of a series of Y-substituted solid solutions of ScF_3 have been reported [4]; these materials are cubic and thermomiotic at room temperature but transition *via* cooperative static rotations of the ScF_6 octahedra into rhombohedral phases with positive thermal expansion upon cooling.

It has previously been suggested that materials with the ReO_3 structure are generally unstable with respect to distortion, largely due to dipole-dipole interactions [5]. Phase transitions potentially related to this instability have been reported in ScF_3 under ≈ 0.1 GPa of pressure at 50 K [2] as well as in $Sc_{1-x}Y_xF_3$, and $Sc_{1-x}Ti_xF_3$ [6]. The phenomenon of transition from a thermomiotic phase to a phase with positive thermal expansion is also seen in many thermomiotic materials from the $A_2M_3O_{12}$ and ABM_3O_{12} families [1], and represents a major challenge to the use of thermomiotic materials in applications. A primary goal of this investigation is to examine the phase transitions in Y-substituted ScF_3 using relaxation calorimetry and confirm the absence of a similar transition in ScF_3 in the absence of applied pressure.

We report herein a low-temperature calorimetric study of ScF_3 and Y-substituted ScF_3 ($Sc_{1-x}Y_xF_3$, $0.05 \leq x \leq 0.25$). The heat capacity of ScF_3 has not previously been reported below room temperature, and it presents additional insight into its phononic and thermodynamic

properties. Specifically, the low-frequency modes which lead to negative thermal expansion have been shown to lead to a peak in the heat capacity expressed as $C_P T^{-3}$ which is absent from conventional, positive thermal expansion materials [1].

We have also calculated *via* density functional theory (DFT) the heat capacity of ScF_3 for comparison, as well as the elastic tensor. The heat capacity calculated using the whole Brillouin zone (BZ) was compared with that calculated knowing only the phonon frequencies at the Γ point. This comparison was performed in order to assess the potential of using a simplifying assumption: that, using the Einstein equation to predict the heat capacity of the optic modes based on their frequencies at Γ and the Debye equation to predict the heat capacity of the acoustic modes, a reasonable estimate of the heat capacity of thermomiotic materials can be obtained. This could be useful, for example, in situations where the heat capacity must be estimated to convert thermal diffusivity into thermal conductivity [7], and would require significantly less computational expense for large systems. The effect of dispersion on heat capacity was previously investigated in $Y_2Mo_3O_{12}$ and was found to play a small but significant role [8].

Materials and Methods:

$Sc_{1-x}Y_xF_3$ (x = 0.05, 0.10, 0.20, and 0.25) were prepared by the solid-state reaction at 1338 K of ScF_3 and YF_3 (both American Elements, 99.99%) in arc-welded Ni ampoules sealed in evacuated quartz tubes as previously described [6]. Lattice constants and sample purity were determined at ambient conditions with a Scintag X1 powder X-ray diffractometer (Cu Kα source and Peltier-cooled solid state detector). The diffraction patterns (Figure 1) were analyzed via the Rietveld method with *GSAS* [9,10] using a cubic structural model (space group $Pm\bar{3}\,m$), and the

lattice constants are given in Table 1. The solid solution samples and a sample of ScF_3 were then pressed (2.0 GPa) and sintered at 1338 K in vacuum. The phase purity of the ScF_3 and $Sc_{0.90}Y_{0.10}F_3$ samples was rechecked by PXRD following sintering.

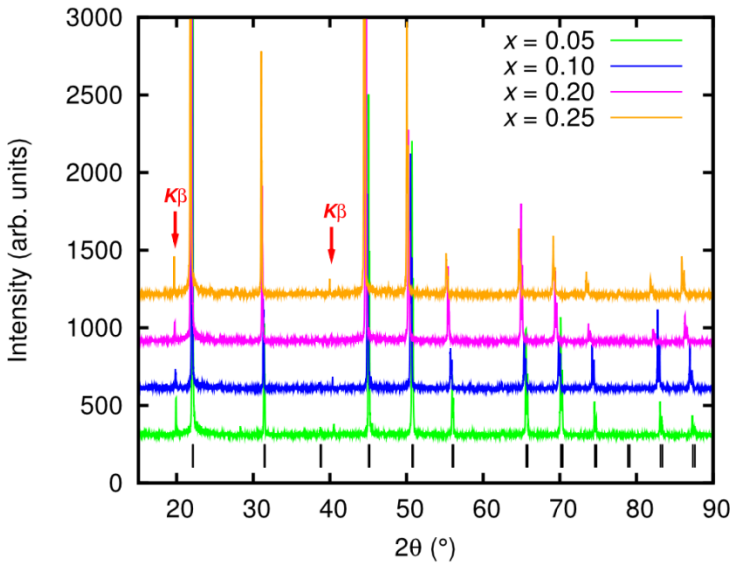

Figure 1: Powder X-ray diffraction (PXRD) patterns collected at ambient conditions on a laboratory diffractometer (Cu Kα radiation) for $Sc_{1-x}Y_xF_3$ samples used for heat capacity measurements. The most prominent Kβ peaks from the X-ray tube are marked by red arrows, and Bragg peaks from the samples are indicated by black tick marks. See the Supplementary Material for an example Rietveld fit [11].

Table 1: Ambient cubic lattice constant, a, of $Sc_{1-x}Y_xF_3$ samples used for heat capacity measurements, determined from Rietveld analysis of PXRD data with a cubic model.

x	a (Å)	esd(a)
0.05	4.021369	0.000148
0.10	4.035079	0.000093
0.20	4.058517	0.000098
0.25	4.072575	0.000096

The heat capacities of ScF_3, $Sc_{0.95}Y_{0.05}F_3$, $Sc_{0.90}Y_{0.10}F_3$, $Sc_{0.80}Y_{0.20}F_3$, and $Sc_{0.75}Y_{0.25}F_3$ were measured using a commercial relaxation calorimeter (Physical Property Measurement System model 6000 from Quantum Design), which can give heat capacity accurate to within 1% for 5 K < T < 300 K and 5% for 0.7 K < T < 5 K [12,13]. Pressed-pellet samples (≈ 1 mm thick) were broken into small shards (< 3×3 mm) and affixed to the measurement platform with a grease serving as the thermal couplant. Heat capacities were measured from 2 K to 300 K using a ^{4}He cryostat and Apiezon® N grease; from 275 K to 390 K using a ^{4}He cryostat and Apiezon® H grease; and from 0.35 K to 10 K using a ^{3}He cryostat and Apiezon® N grease. All reported data points met reliability criteria (≥ 90% thermal coupling constant between sample and platform and ≥ 40% sample contribution to the total heat capacity). Data tables and sample masses are presented in the Supplementary Material [11].

DFT calculations were carried out using the ABINIT code with pseudopotentials and plane waves [14,15]. Norm-conserving pseudopotentials generated by the OPIUM code [16] were used as received from the Bennett and Rappe Pseudopotential Library [17]. Perdew–Burke–Ernzerhof exchange-correlation functionals were used [18]. These functionals were compared to local density approximation functionals and found to give a value of the bulk modulus of ScF_3 closer to the experimental value (≈ 60 GPa) [2,4]. We have chosen this point of comparison because experimental results suggest that the bulk modulus of ScF_3 is largely independent of

temperature between 300 and 500 K [4] (unlike some other thermomiotic materials such as ZrW_2O_8 [19] and HfW_2O_8 [20] for which the bulk modulus is strongly temperature dependent), which would facilitate direct comparison with first principles calculations. Additionally, the temperature-dependent phonon spectrum experimentally obtained by inelastic neutron scattering shows little change in the energy of the low-energy phonons with temperature [3].

The experimental lattice constant (the only structural parameter of ScF_3 unrestricted by symmetry) was relaxed until the maximum stress in the cell was below 10^{-7} hartree/bohr^3, resulting in an increase of the lattice constant by 1.4 % and a final internal pressure of 1.06×10^{-3} GPa. Calculation of the electronic structure of ScF_3 was then performed using a 50 hartree plane-wave-energy cut-off and a $6 \times 6 \times 6$ shifted Monkhorst–Pack grid [21] of reciprocal space vectors. This grid size corresponds to a spacing of points of 0.042 Å^{-1}. Subsequently, the responses to electric fields, atomic displacements and strains were computed using the response-function functionality of ABINIT; the atomic displacements were computed over a $6 \times 6 \times 6$ grid of reciprocal space vectors. The dynamical matrices resulting from these calculations were then used to calculate the stiffness tensor and interpolated over an $80 \times 80 \times 80$ grid of reciprocal space vectors to compute the phonon dispersion relation and the heat capacity (see Supplementary Material for data [11]). The stiffness tensor was calculated to determine the Debye temperature, to compare the bulk modulus (K) to experiment, and to determine the heretofore unreported shear modulus (G), Young's modulus (E), and Poisson ratio (v) of ScF_3.

For comparison, the heat capacity was also calculated using only the phonon frequencies at Γ and the Debye temperature (θ_D). The heat capacity of the optic bands was calculated treating each optic mode as an independent Einstein oscillator while the heat capacity due to the acoustic bands was calculated using the Debye equation. The Debye temperature was obtained from the

elastic constants using a geometric Voigt–Reuss–Hill (VRH) average [22], which generally produces the most accurate estimates of the Debye temperature for polycrystalline aggregates [22].

Results and Discussion:

The calculated stiffness tensor, ***c***, of ScF_3 has the following unique elements: c_{11} = 230 GPa, c_{12} = 17.3 GPa, c_{44} = 18.0 GPa. The geometric VRH values for the isotropic elastic constants are K = 88.4 GPa, G = 38.0 GPa, E = 99.1 GPa and ν = 0.30 [22]. This leads to a value of 505 K for θ_D. Interestingly, there is a large difference between the Voigt (uniform strain) and Reuss (uniform stress) values for the shear modulus, with G_V = 53.4 GPa and G_R = 27.1 GPa. Because $G_V = G_R$ for an isotropic solid, the large difference can be interpreted as an indication of elastic anisotropy in this cubic material. The origin of this anisotropy can be understood by considering the difference between a force applied along [100], where there are Sc–F–Sc chains, and a force applied along [111], where there are isolated Sc^{3+} ions. This result is consistent with the large role dispersion plays in the thermal properties of ScF_3 (*vide infra*).

The calculated phonon dispersion relation and the phonon density of states (DOS) of ScF_3 are presented in the Supplementary Material [11]. The DFT-calculated phonon dispersion and DOS have been previously reported and compared to inelastic neutron scattering results [3]; we have carried out similar calculations in order to calculate the heat capacity and elastic properties of ScF_3, not previously reported.

The molar heat capacity at constant pressure (C_P) of ScF_3 as measured experimentally was converted to molar heat capacity at constant volume (C_V) using literature values for the compressibility and temperature-dependent CTE [4]. The result is plotted along with the DFT C_V

result in Figure 2. The molar volumes for the C_V value from DFT and the experimental C_V are normally slightly different: the former is constant, and the latter allows for different volumes at different temperatures. Nevertheless, C_V values can be directly compared in this case because the compressibility and coefficient of thermal expansion of ScF_3 are largely invariant with volume [4].

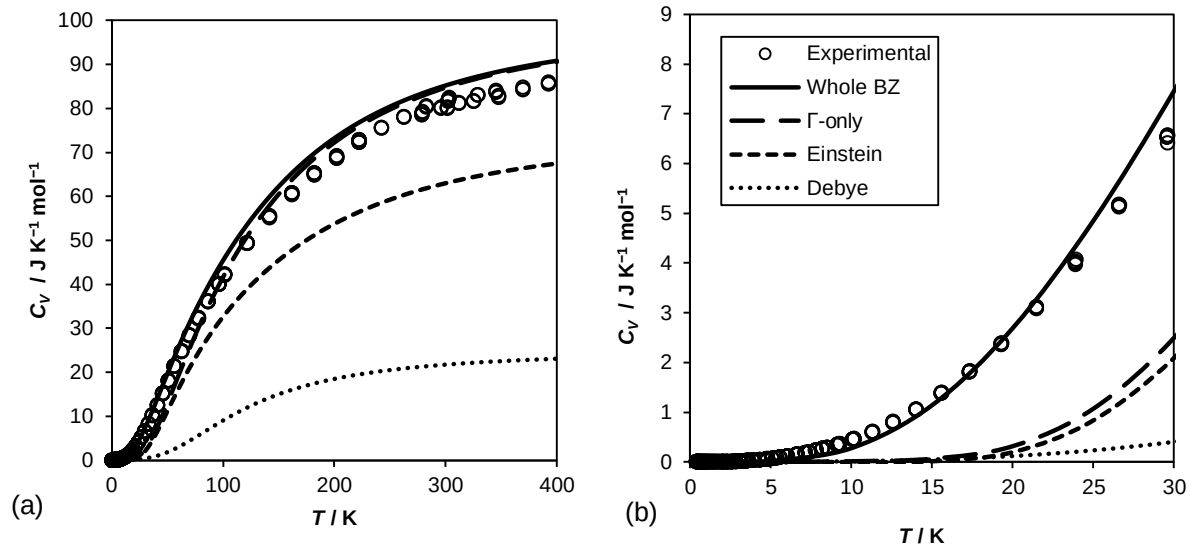

Figure 2: The molar constant-volume molar heat capacity of ScF_3 as a function of temperature as determined from experiment, as calculated using the whole Brillouin zone, and as calculated using the sum of the Einstein models of the phonon frequencies at the Γ point and the Debye contribution from the acoustic modes (a) over a wide temperature range, and (b) at low temperature. The Einstein calculation of the heat capacity of the optic modes and the Debye calculation of the heat capacity of the acoustic modes are also shown.

The full-BZ DFT calculations of the heat capacity provide an excellent match to the experiment in the temperature range from 15 to 400 K, but diverge significantly below this temperature (see Figure 3). Comparison of the calculated phonon DOS [11] with the experimental DOS reported from inelastic neutron scattering [3] shows that there are fewer states in the calculated DOS at the lowest energies. The differences between experiment and the full-BZ calculation in the heat capacity below 15 K could possibly be due to quartic anharmonicity of transverse motions of the F atoms, which has been reported to significantly influence the low-

temperature thermal expansion of ScF_3 [3], since the DFT calculations are confined to the harmonic approximation. Previously reported frozen-phonon calculations showed softening of the potential of the R4+ mode when a quartic model was used [3]. Since this anharmonic behaviour is expected to be general to the low-energy rigid-unit modes near R [3], the reduction in their energies would lead to an increase in the low-temperature heat capacity above that predicted by the harmonic approximation. In order to investigate this discrepancy further, additional frozen-phonon or molecular dynamics calculations on supercells should be performed to better understand the effect of anharmonicity on the low-temperature phononic properties of ScF_3.

Additionally, we have calculated the acoustic band between R and M to be nearly dispersionless [11]. The calculated energy of the acoustic band at R is higher than that reported in [3]. If the present calculations overestimate the energy of the acoustic band at R, it would lead to an underestimation of the low-temperature heat capacity.

The low-temperature heat capacity of ScF_3 is of interest because the presence of low-dispersion low-frequency modes is highly correlated with negative thermal expansion, for example in HfW_2O_8 [23] and $Zn(CN)_2$ [24], as these modes often correspond to coordinated rotation of rigid units. Many thermomiotic materials have low-energy vibrational modes that are not well-described by the Debye model, which manifest as a low-temperature peak in $C_P T^{-3}$ (Figure 3). Similar peaks have previously been reported in other thermomiotic materials, although they are usually attributed more to the contribution of low-energy optic bands than to the non-Debye-like behaviour of the acoustic bands [8,25,26,27,28]. When expressed per mole of atoms rather than per mole of formula units, the height of the peak in $C_P T^{-3}$ of ScF_3 is similar in magnitude to reports for other thermomiotic materials (0.15 mJ K^{-4} mol^{-1}; *cf.* $Y_2Mo_3O_{12}$, 0.4 mJ

K^{-4} mol^{-1} [8]; ZrW_2O_8, 0.3 mJ K^{-4} mol^{-1} [25]; $HfMo_2O_8$, 0.2 mJ K^{-4} mol^{-1} [27]; and $Sc_2W_3O_{12}$, 0.2 mJ K^{-4} mol^{-1} [28]), indicating directly from experimental heat capacity data that there are low-energy vibrational states with negative Grüneisen parameters available in ScF_3.

The Γ-only calculations dramatically underestimate the heat capacity at low temperatures (especially T < 100 K), indicating that dispersion plays an important role in the low-temperature heat capacity of ScF_3. The Debye contribution underestimates the acoustic modes at low temperatures due to their unusually low energies near the R and M points [11]. Additionally, there are low-frequency optic modes with negative Grüneisen parameters that contribute to the heat capacity at low temperature [3]. Therefore, ScF_3 behaves thermally at low temperatures as if the lattice is much less stiff than is implied by the elastic constants, due to the vibrational modes that are responsible for NTE.

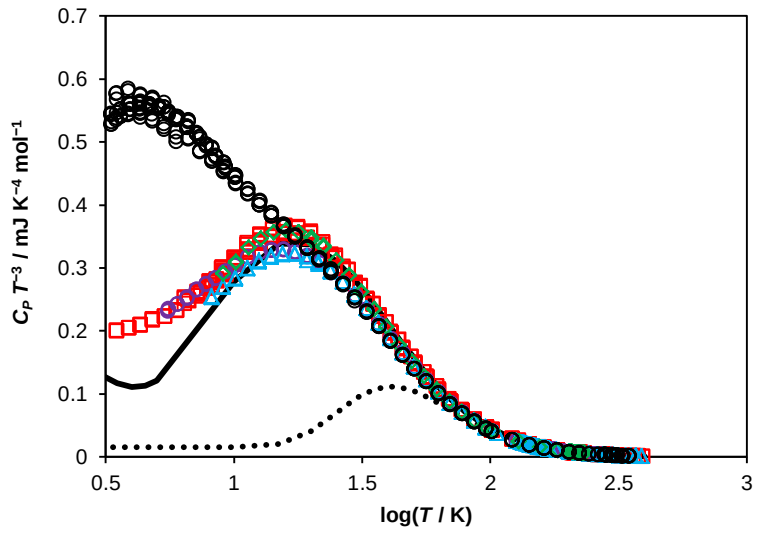

Figure 3: The experimental molar heat capacity of ScF_3 (○), $Sc_{0.95}Y_{0.05}F_3$ (○), $Sc_{0.9}Y_{0.1}F_3$ (△), $Sc_{0.8}Y_{0.2}F_3$ (◇), and $Sc_{0.75}Y_{0.25}F_3$ (□), expressed as $C_P T^{-3}$, as a function of temperature, and for ScF_3 as calculated using the whole Brillouin zone (solid black line), and as calculated without dispersion using the optic phonon frequencies at the Γ point and the Debye temperature (dotted black line) (colour online).

Experimentally-determined heat capacities of four $Sc_{1-x}Y_xF_3$ solid solutions are shown in Figures 3 and 4; complete data tables are available in the Supplementary Material [11]. The molar heat capacities of Y-substituted ScF_3 are close to that of ScF_3 in their cubic (room temperature) phases; however, upon cooling, they transition between 250 K and 100 K (transition temperature varies with composition) to rhombohedral phases [4], at which point their heat capacities begin to diverge from that of ScF_3. The low-temperature heat capacities of the Y-substituted materials are smaller than for ScF_3 (Figures 3 and 4 (c)), which correlates with the positive thermal expansion of the rhombohedral phases.

Although the heat capacity of ScF_3 is larger than that of the Y-substituted materials at low temperature, significant peaks are visible in the heat capacities of the latter expressed as $C_P T^{-3}$ (Figure 3), which is atypical for positive thermal expansion materials [1]. However, a similar result was previously reported in the heat capacity of the framework material $HfMgMo_3O_{12}$, which has low positive thermal expansion at room temperature, undergoes a pseudo-second-order transition into a monoclinic phase upon cooling [26], but still shows a significant peak in $C_P T^{-3}$ in this low-temperature phase [26]. $Sc_2Mo_3O_{12}$, a thermomiotic material at room temperature, also undergoes a transition into a positive thermal expansion phase upon cooling and shows a peak in $C_P T^{-3}$ at low temperature [28]. Presumably, some of the low-frequency modes with negative Grüneisen parameters can persist following low-energy displacive phase transitions of framework materials even when the material as a whole exhibits a positive CTE. Experimental identification of the changes in the phononic structure related to the phase transition in the solid solutions and their influence on the thermal expansion would require variable-pressure, variable-temperature inelastic neutron scattering. Although computational investigation of such a disordered system is possible in principle, for example using a special

quasirandom structure model [29] to determine the phononic structure of rhombohedral $Sc_{1-x}Y_xF_3$, in practical terms to incorporate the Y-doping and the subsequent structural distortions would require the use of a unit cell much larger than that of ScF_3, considerably increasing the resources required.

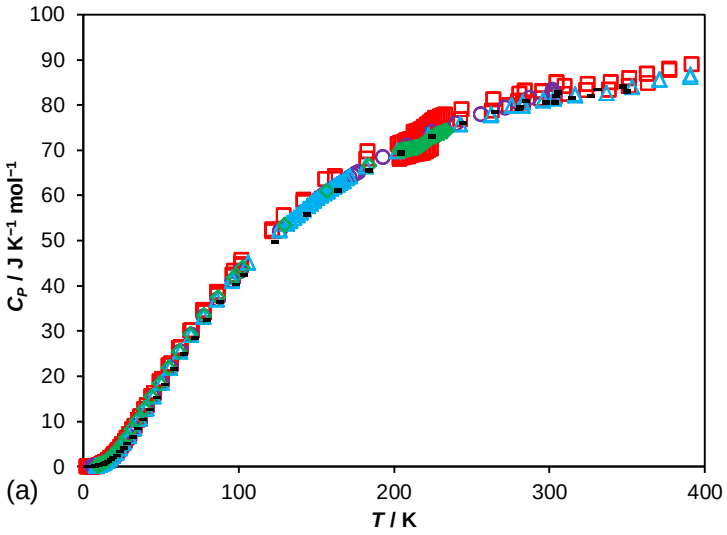

(a)

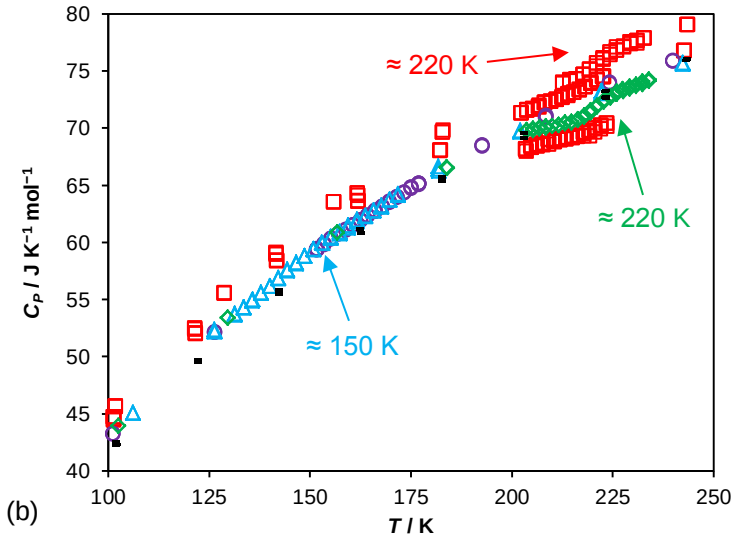

(b)

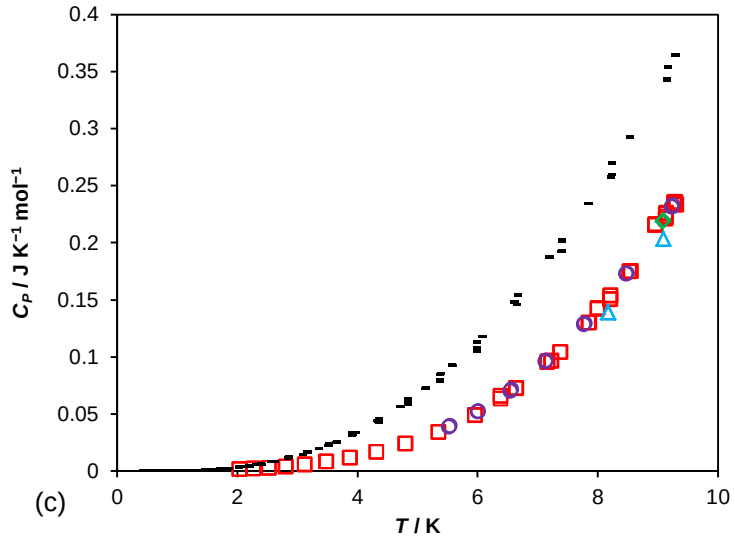

Figure 4: The experimentally measured molar heat capacities of $Sc_{0.95}Y_{0.05}F_3$, (○) $Sc_{0.9}Y_{0.1}F_3$, (△) $Sc_{0.8}Y_{0.2}F_3$ (◇), $Sc_{0.75}Y_{0.25}F_3$ (□), and ScF_3 (-) as a function of temperature: (a) full temperature range view; (b) phase-transition temperature region (with estimated cubic-rhombohedral phase transition temperatures indicated), and (c) low-temperature region (colour online). See the Supplementary Materials for derivatives of the heat capacity in the phase transition regions [11].

Cubic-rhombohedral phase transitions can be observed (Figure 4 (b)) in the heat-capacity data for $Sc_{0.8}Y_{0.2}F_3$ and $Sc_{0.75}Y_{0.25}F_3$ at approximately 220 K and very weakly for $Sc_{0.9}Y_{0.1}F_3$ at 150 K. These temperatures are somewhat higher than those reported from variable-temperature XRD [4]; however, they are close to the inflection point in the reported volume-temperature curve. The small anomalies in heat capacity are consistent with second-order phase transitions, as suggested by the XRD data [4]. A phase transition was not observed in the heat capacity of $Sc_{0.95}Y_{0.05}F_3$; possibly it was below the detection limit. A low enthalpy change is consistent with the low-temperature heat capacity results: the relatively high values of the low-temperature heat capacity suggest that the Y-doped ScF_3 solid solutions have considerable vibrational entropy in their rhombohedral phases [30], stabilizing them with respect to the cubic phase, which in the case of ScF_3 also has considerable vibrational entropy.

There is no experimental evidence of a phase transition in ScF_3 at any point in the temperature range studied (0.38 K to 390 K). The low-temperature heat capacity of ScF_3 is significantly higher than that of the Y-substituted materials down to the lowest temperature measured for those samples (2.03 K for $Sc_{0.75}Y_{0.25}F_3$). This finding is consistent with the absence of negative-frequency vibrational modes in the DFT $T = 0$ K phonon structure, which would be indicative of structural instability. The present experimental and theoretical results, in combination with previously reported low-temperature diffraction experiments [2,3,4], suggest that ScF_3, in the absence of applied pressure, is not susceptible to the distortional instability identified in other ReO_3 structures [5].

Conclusions:

The experimental heat capacity of ScF_3 from 0.38 to 390 K shows no evidence of a phase transition. The low-temperature heat capacity of ScF_3 shows significant deviation from the Debye model, which was shown from the calculated phonon dispersion to be due to the low-energy phonon modes that are responsible for negative thermal expansion in ScF_3. We also report the heat capacities of $Sc_{0.95}Y_{0.05}F_3$, $Sc_{0.9}Y_{0.1}F_3$, $Sc_{0.8}Y_{0.2}F_3$, and $Sc_{0.75}Y_{0.25}F_3$; the last three show evidence of a cubic-rhombohedral phase transition as previously reported. The low-temperature heat capacities of the rhombohedral phases have a smaller low-temperature anomaly, in terms of $C_P T^{-3}$, than ScF_3.

ACKNOWEDGEMENTS

This study was supported by the Natural Sciences and Engineering Research Council of Canada, the Sumner Foundation, and the Canada Foundation for Innovation, the Atlantic Innovation Fund and other partners that fund the Facilities for Materials Characterization managed by the Institute for Research in Materials at Dalhousie University.

References:

[1] Romao CP, Miller KJ, Whitman CA, White MA, Marinkovic, BA (2013) Negative thermal expansion (thermomiotic) materials. In: Reedijk J, Poppelmeier K (eds) Comprehensive Inorganic Chemistry vol 4. Elsevier, Oxford pp 128–151.
[2] Greve BK, Martin, KL, Lee PL, Chupas PJ, Chapman KW, Wilkinson AP (2010) Pronounced negative thermal expansion from a simple structure: cubic ScF_3, J Am Chem Soc 132:15496–15498.
[3] Li CW, Tang X, Muñoz JA, Keith JB, Tracy SJ, Abernathy DL, Fultz B (2011) Structural Relationship between Negative Thermal Expansion and Quartic Anharmonicity of Cubic ScF_3, Phys Rev Lett 107:195504-1–195504-5.
[4] Morelock CR, Greve BK, Gallington LC, Chapman KW, Wilkinson AP (2013) Negative thermal expansion and compressibility of $Sc_{1-x}Y_xF_3$ ($x \leq 0.25$), J Appl Phys 114:213501-1–213501-8.
[5] Allen PB, Chen YR, Chaudhuri S, Grey CP (2006) Octahedral tilt instability of ReO_3-type crystals, Phys Rev B 73:172102-1–172102-4.
[6] Morelock CR, Gallington LC, Wilkinson AP (2014) Evolution of Negative Thermal Expansion and Phase Transitions in $Sc_{1-x}Ti_xF_3$, Chem Mater 26:1936-1940.
[7] White, MA (2012) Physical Properties of Materials. CRC Press, Boca Raton.
[8] Romao CP, Miller KJ, Johnson MB, Zwanziger JW, Marinkovic BA, White MA (2014) Thermal, vibrational, and thermoelastic properties of $Y_2Mo_3O_{12}$ and their relations to negative thermal expansion, Phys Rev B 90:024305-1–024305-9.
[9] Larson AC and Von Dreele RB (2000) General Structure Analysis System (GSAS), Los Alamos National Laboratory: Los Alamos National Laboratory Report LAUR 86-748.
[10] Toby BH (2001) *EXPGUI*, a graphical user interface for *GSAS*, J Appl Cryst 34:210–213.
[11] Supplementary Material at [URL to be inserted by journal].
[12] Kennedy CA, Stancescu M, Marriott RA, White MA (2007) Cryogenics 47, 107 (2007)
[13] Johnson MB and White MA (2014) Thermal Methods. In: Bruce DW, O'Hare D, Walton RI (eds) Inorganic Materials: Multi Length-Scale Characterization ch 2. Wiley, New York pp 63–120.
[14] Gonze X, Amadon B, Anglade P-M, et al. (2009) ABINIT : first-principles approach to material and nanosystem properties, Comput Phys Commun 180:2582–2615.
[15] Gonze X, Beuken J-M, Caracas R, et al. (2002) First-principles computation of material properties: the ABINIT software project, Comp Mater Sci 25:478–492.
[16] http://opium.sourceforge.net
[17] http://www.sasupenn.edu/rappegroup/htdocs/Research/psp_gga.html
[18] Perdew JP, Burke K, Ernzerhof M (1996) Generalized Gradient Approximation Made Simple, Phys Rev Lett 77:3865–3868.
[19] Drymiotis FR, Ledbetter H, Betts JB, Kimura T, Lashley JC, Migliori A, Ramirez AP, Kowach GR (2004) Monocrystal elastic constants of the negative-thermal-expansion compound zirconium tungstate (ZrW_2O_8), Phys Rev Lett 93:025502-1–025502-4.
[20] Gallington LC, Chapman KW, Morelock CR, Chupas PJ, Wilkinson AP (2014) Dramatic softening of the negative thermal expansion material HfW_2O_8 upon heating through its WO_4 orientational order-disorder phase transition, J Appl Phys 115:053512-1–053512-5.

[21] Monkhorst HJ and Pack JD, (1976) Special points for Brillouin-zone integrations, Phys Rev B 13:5188–5192.
[22] Ledbetter HM (1973) Estimation of Debye temperatures by averaging elastic coefficients, J Appl Phys 44:1451–1454.
[23] Mittal R, Chaplot SL, Kolesnikov AI, Loong C-K, Mary TA (2003) Inelastic neutron scattering and lattice dynamical calculation of negative thermal expansion in HfW_2O_8, Phys Rev B 68:054302-1–054302-7.
[24] Zwanziger JW (2007) Phonon dispersion and Grüneisen parameters of zinc dicyanide and cadmium dicyanide from first principles: Origin of negative thermal expansion, Phys Rev B 76: 052102-1–052102-4.
[25] Kennedy CA and White MA (2005) Unusual Thermal Conductivity of the Negative Thermal Expansion Material, ZrW_2O_8, Solid State Commun 134:271–276.
[26] Miller KJ, Johnson MB, White MB, Marinkovic BA (2012) Low-temperature investigations of the open-framework material $HfMgMo_3O_{12}$, Solid State Commun 152:1748–1752.
[27] Jakubinek MB, Whitman CA, White MA (2010) Negative thermal expansion materials: thermal properties and implications for composite materials, J Therm Anal Calorim 99:165–172.
[28] Yamamura Y, Ikeuchi S, Saito K (2009) Characteristic Phonon Spectrum of Negative Thermal Expansion Materials with Framework Structure through Calorimetric Study of $Sc_2M_3O_{12}$ (M = W and Mo), Chem Mater 21:3008–3016.
[29] Zunger A, Wei S-H, Ferreira LG, Bernard JE (1990) Special Quasirandom Structures, Phys Rev Lett 65:353–356.
[30] Fultz B (2010) Vibrational thermodynamics of materials, Prog Mater Sci 55:247–352.